Technical Report No. 32-527

Degradation of Homogeneous Polymeric Materials Exposed to High Heat Fluxes

Robert G. Nagler

JET PROPULSION LABORATORY
CALIFORNIA INSTITUTE OF TECHNOLOGY
PASADENA, CALIFORNIA

February 1, 1964

(NASA Contract NAS7-100)

(NASA CR-53256 ; JPL-TR-32527) OTS: $2.60 ph, $1.10 mf

(JPL TR

~~Technical Report No. 32-527~~

Degradation of Homogeneous Polymeric Materials Exposed to High Heat Fluxes

Robert G. Nagler 1 Feb. 1964 30 p refs

[2]

☒ OTS

L. D. Jaffe, Chief
Materials Research Section

JET PROPULSION LABORATORY
CALIFORNIA INSTITUTE OF TECHNOLOGY
PASADENA, CALIFORNIA

February 1, 1964

Prepared Under Contract No. NAS 7-100
National Aeronautics & Space Administration

CONTENTS

TABLES

FIGURES

FIGURES (Cont'd)

ABSTRACT

17494 A

An arc imaging furnace was used to expose polymeric materials to a variety of heating rates under static or near-static flow conditions and under reduced pressures. Data obtained on polymethylmethacrylate, polytetrafluoroethylene, and polyethylene show a linear relationship between heat input and surface recession which is not inconsistent with theory. Comprehensive measurements of polymer reflectivities and transmissivities are necessary before a detailed analysis of the data would be meaningful. The degradation products collected in this investigation do not agree with those previously reported for these polymers at similar temperatures and heating rates. Author

I. INTRODUCTION

At the present time, much attention is being given to polymeric materials, both with and without secondary reinforcements, for use in ablative situations such as Earth re-entry (Ref. 1), planetary entry (Ref. 2), rocket exhaust systems (Ref. 3), etc. Most of this work is being done without rigorous scientific appraisal to determine why a particular material does or does not survive in a particular use situation. In the early stages of a comparatively new field of interest, such random study is often advantageous. When the initial breakthroughs due to gross screening of the available materials are completed, it becomes necessary to develop more rigorous methods of analysis to discover why certain materials are advantageous over others, and what new materials can be made to provide even better properties.

One approach, under consideration by the Materials Research Section of the Jet Propulsion Laboratory, is to study the stability of some of the simpler organic polymeric materials under a variety of energy-input methods and rates, at various temperatures and pressures (including highly ionized systems), and under both static and dynamic flow conditions. Testing in such a program would include:

1. High-vacuum evaporation studies at temperatures up to and including the degradation or ceiling temperature of the polymer studied.
2. Vaporization studies at high and low heating rates (a) in a static system or systems, (b) in a dynamic system without ionization, (c) in a dynamic system

with primarily chemical ionization, and (d) in a dynamic system with both chemical and thermal ionization.

3. Measurements of physical and optical properties.

Initially, the investigation would be limited to thermoplastics, which are more easily characterized and better understood. All data taken in such a testing program would be compared as to the molecular structure and the available physicochemical properties of the tested materials. The purpose of the investigation would be to develop "building blocks" to aid in a better understanding of the more complicated polymers and polymer composites.

The study reported here concerns the decomposition or degradation of thermoplastics under purely radiant energy, with heat fluxes in the range of 100 to 1000 Btu/ft^2-sec. The degradation was studied under static or near-static flow conditions in various atmospheres and at pressures in the range of 1 atm to 1 μ. Products and residues from the degradation process were collected and analyzed.

II. TEST PROGRAM

A. Test Equipment

A schematic diagram of the entire experimental setup is shown in Fig. 1, and a photograph of the actual equipment in Fig. 2. A commercial arc imaging furnace[1], shown at the left in Fig. 1, serves as the radiant-energy source. The furnace uses an air-blown arc source, powered by a dry-rectifier power supply with 160- and 300-amp output settings. The blown arc is given added stabilization by use of a plasma-stirring solenoid, and the power-level fluctuations are held to about 6% by use of a special anode and cathode feed mechanism. Cored carbon anodes provide a high-intensity cup. The image of this source is projected from the minor focus of one 21-in. ellipsoidal mirror and is collected and reimaged by a second similar ellipsoidal mirror. For the vertical operation used in this investigation, a water-cooled flat 45-deg mirror was inserted in the major focal cone of the reimaging mirror.

Specimen location is controlled by a special motor-driven positioner arm, which may be moved in each of the three axial directions. The specimen holder and the 4-in.-diameter hemispherical Pyrex domes for vacuum and controlled-atmosphere tests are shown in Figs. 3 and 4. High-temperature silicone-base vacuum greases are used to seal the domes to a flat Pyrex plate. A thin, highly polished aluminum plate is attached to the back of the specimen-positioning arm in direct focal line with the specimen holder. This plate reflects the energy normally impinging on the specimen holder, preventing the holder from warming too rapidly during test operations.

Exposure time is controlled by a manually operated shutter in the major focal cone of the projection mirror. For this investigation, the effect of finite opening and closure time was ignored. An electrical timer is actuated when the shutter blocks half of the radiant beam.

The degradation-product collection and fractionation apparatus is shown at the right in Fig. 1. The apparatus is similar to that used by Friedman (Ref. 4). Two collection systems are set up in parallel to allow collection of the gaseous degradation products from two parts of a single long run or from consecutive runs on a single material. A single collection system consists of two liquid nitrogen traps, a surge volume, and a blowout manometer. The two traps are necessary to permit the collection of more than 99% of the condensible materials entering the traps. For most runs, the surge volume is used to reduce pressure fluctuations from the pump and to take

[1] Arthur D. Little, Inc.

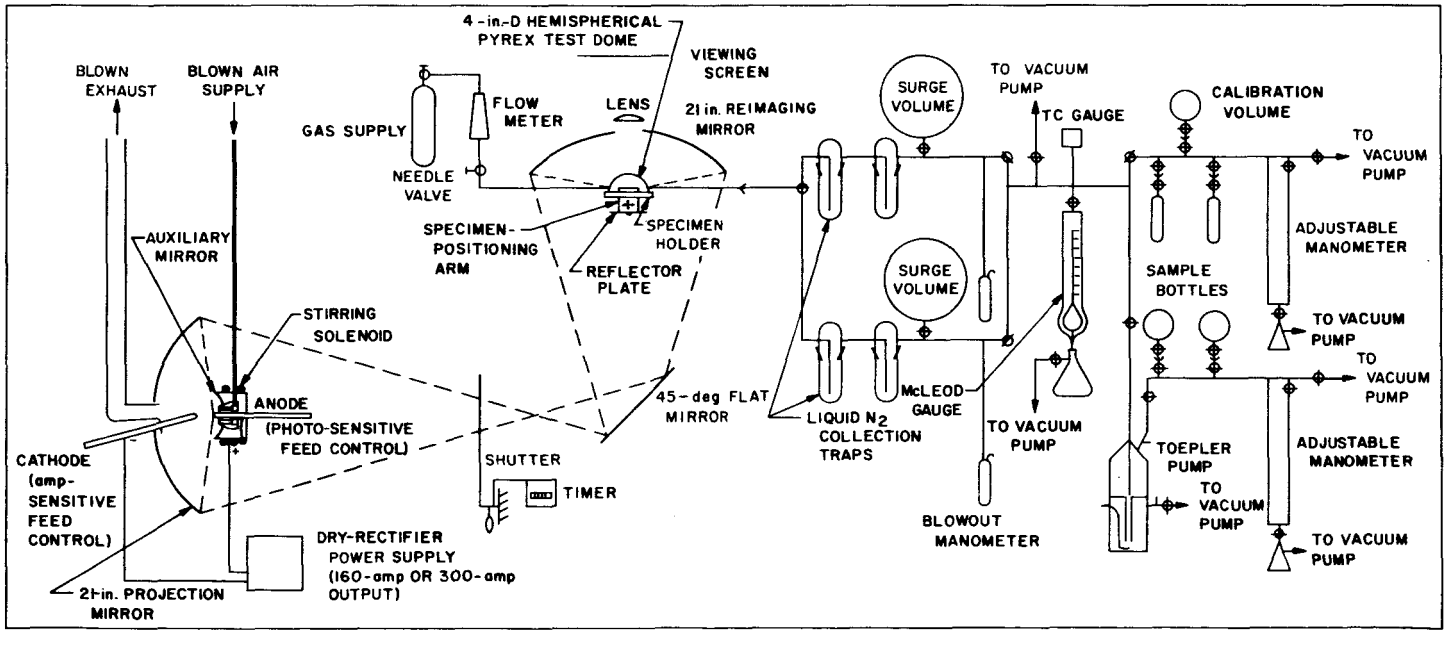

Fig. 1. Schematic diagram for studies of polymer degradation at variable heat fluxes

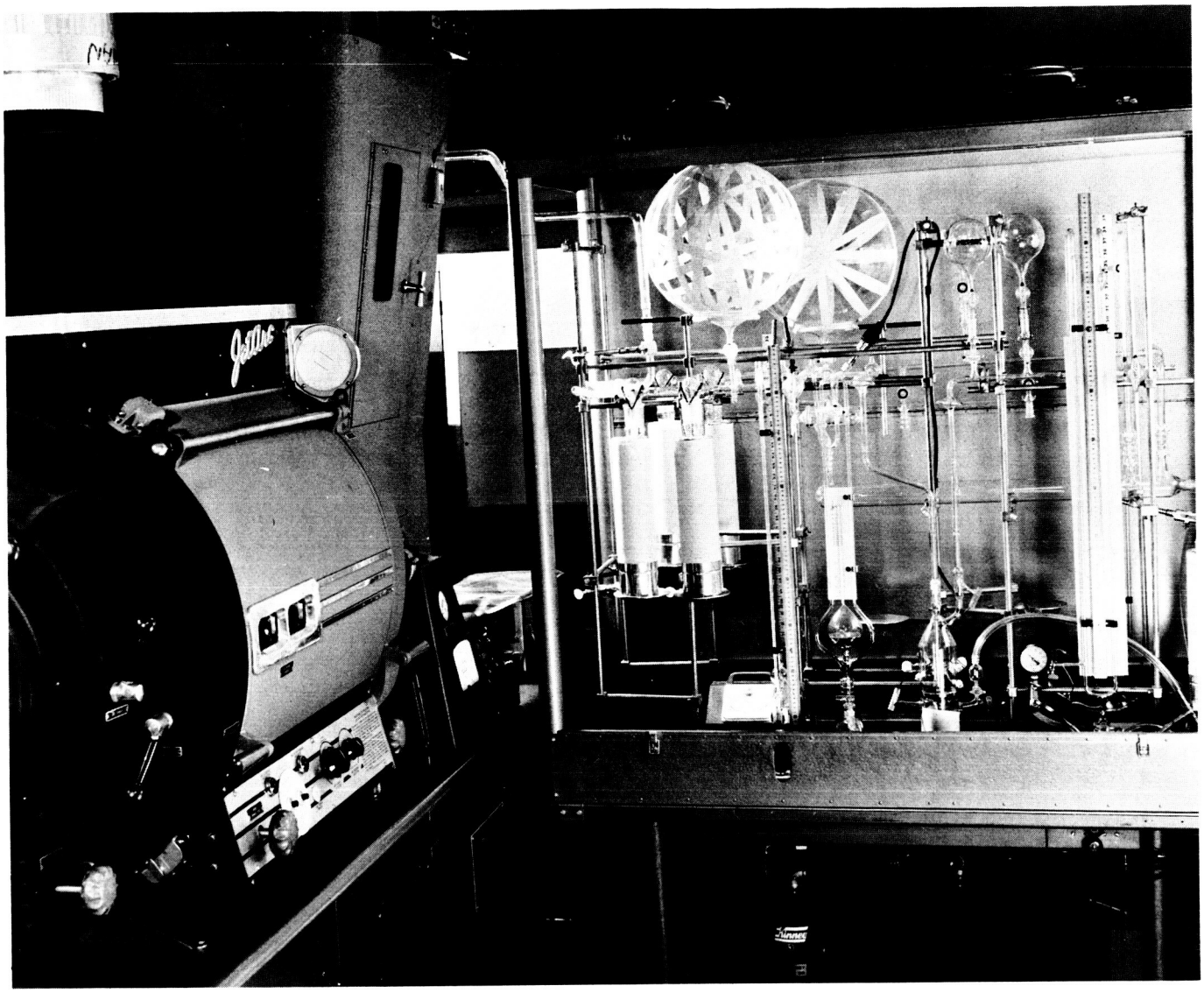

Fig. 2. Arc imaging furnace and polymer-degradation collection and fractionation apparatus

up the pressure from the evolution of hydrogen or other low-molecular-weight gases. On runs where the surge volume is not used, and mechanical pumping is done throughout the test, the second liquid nitrogen trap is loosely packed with glass wool to minimize the amount of the condensibles passing through both traps. This is not done in the runs using the surge volume, because the glass wool can trap or absorb some of the condensibles, slowing down and, in part, preventing completion of the later fractionation process. The blowout manometer may be used to monitor pressure changes due to the evolution of large amounts of low-molecular-weight noncondensible gases during the degradation process. It also acts as a safety device by limiting the maximum pressure.

Pressures in the collection and fractionation system are monitored down to 10^{-3} mm Hg with a standard thermocouple gauge and a low-pressure McLeod gauge. For runs where pressures between atmospheric and 1 mm Hg are necessary, a calibrated Bourdon-tube gauge is connected directly to the dome assembly.

The fractionation portion of the apparatus is divided into two sections. One section uses a Toepler pump to collect low-molecular-weight noncondensibles. This section contains two specimen-collection connections and an adjustable manometer for volume measurements. The second section is set up to use distillation techniques to separate the higher-molecular-weight gases into as many

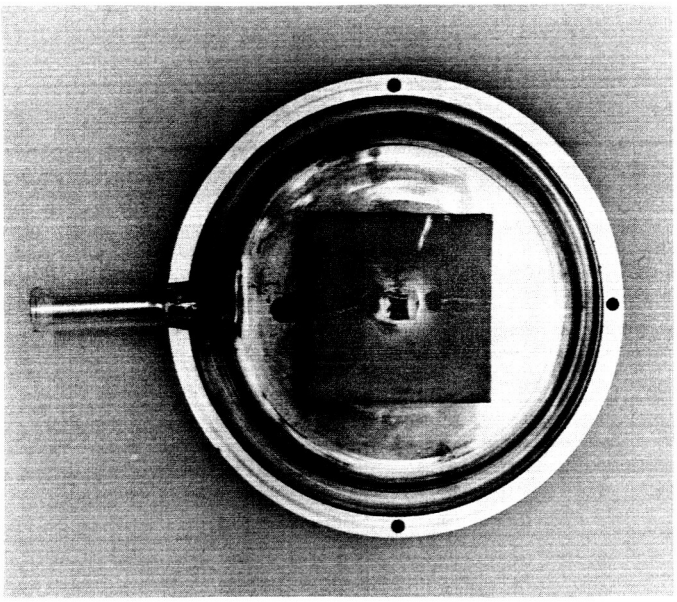

Fig. 3. Specimen holder and 4-in.-diameter hemispherical dome for vacuum studies

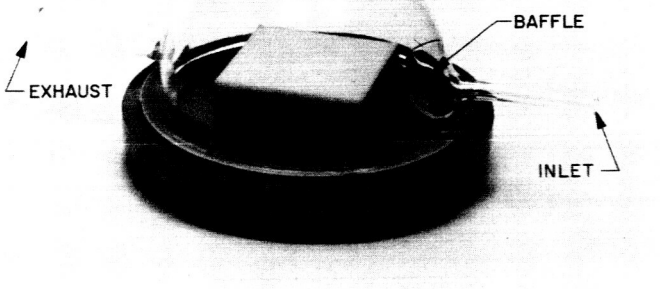

Fig. 4. Specimen holder and 4-in.-diameter hemispherical dome for controlled-atmosphere studies

fractions as are desirable or convenient. This section contains suitable bottle connections and another adjustable manometer to measure the volumes of the distilled gases.

An 8-ft^3/min-capacity compound vacuum pump, protected by a large glass-wool-filled liquid nitrogen trap, is used to pump the main portions of the collection and fractionation apparatus. Control vacuums for the McLeod gauge, Toepler pump, and adjustable manometers are furnished by a separate vacuum pump with a 3-ft^3/min capacity.

B. Heat-Flux Calibration

Heat-flux calibration in the apparatus described above consists of measuring the heat flux at any point within a 1-in.-diameter sphere centered at the minor focal point of the reimaging mirror. A water-cooled Gardon foil-type radiometer with a 1-mm-diameter (0.00487-in.^{2}) blackened spot was used to determine the flux distribution (see Fig. 5).

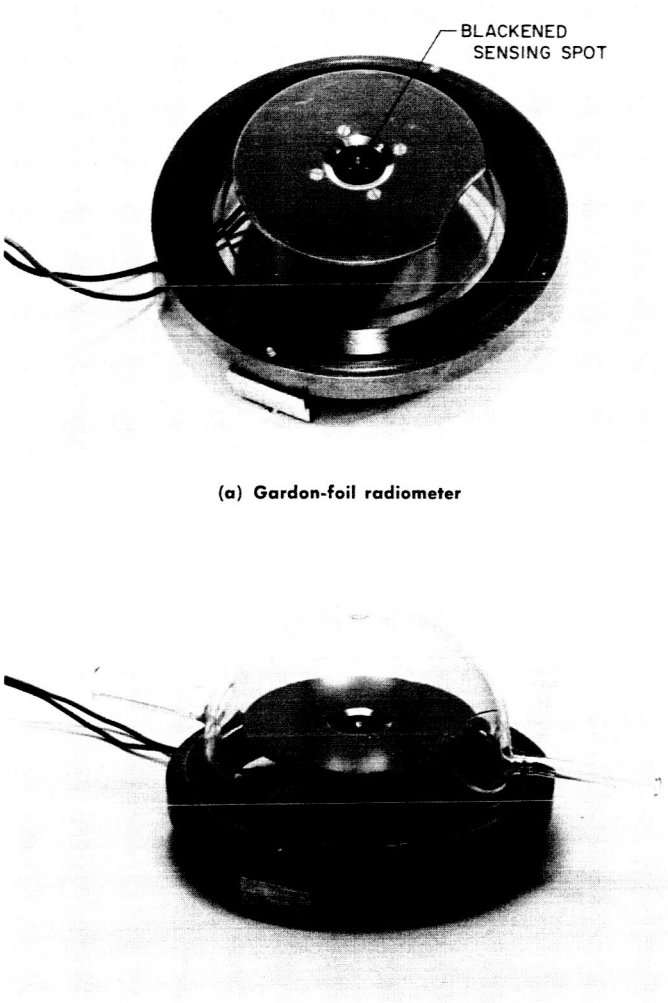

(a) Gardon-foil radiometer

(b) Radiometer under hemispherical test dome

Fig. 5. Radiometer used for determination of flux distribution

Calibration of the radiometer for a particular cooling-water flow rate was accomplished by equating the heat flux to a blackened water-cooled copper calorimeter exposed to the arc, with radiometer output readings integrated over the same area. A standard commercial calo-

rimeter, Fig. 6(a), and a JPL-developed calorimeter, Fig. 6(b), were found to give the same initial calibration. Each of the calorimeters uses a water-cooled copper jacket around the sensing area (0.104 in.^{2} for the commercial model, and 0.0620 in.^{2} for the JPL model). The radiometer must be recalibrated every time it is used to measure heat fluxes, unless the cooling-water temperature and flow rate are held constant.

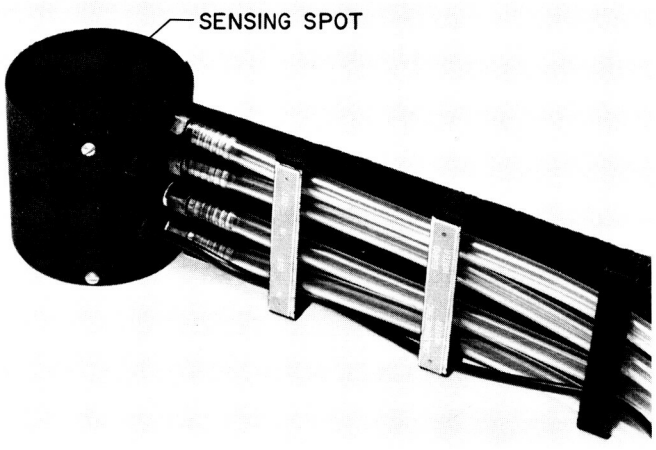

(a) Commercial calorimeter

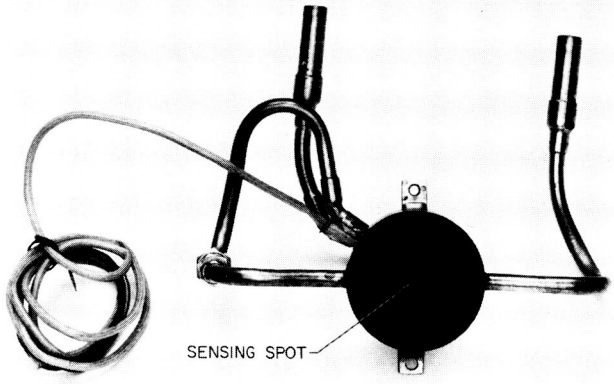

(b) JPL-developed calorimeter

Fig. 6. Calorimeters used for radiometer calibrations

Several radiometer traverses were taken in the focal plane in four perpendicular directions extending out from the focal point. Using the motor-driven positioner arm, continuous traverses were taken and were matched with stepped traverses in which the arc was started and run for several minutes for each new position of the radiometer. All the data from each of the four traverses were averaged, and each of the resultant curves was assumed to represent one-quarter of the total flux distribution. The total heat flux of each quarter was determined by graphical integration over the same area as that sensed by the calorimeter. The sum of the heat fluxes from the four quarters was then equated to the average heat flux measured with the calorimeter.

Both the flux averaging mentioned above and the flux ranges, which are discussed later, were necessary because of a characteristic of the power supply for this blown-arc system. During approximately the first minute of operation, the heat flux increased slowly about 10%. At the end of this time, a maximum flux was achieved. The flux then decreased at a steady rate for about 4 min. When about half of the original 10% rise had been lost, the loss rate decreased, and the flux began to level out slowly to a constant value. Unfortunately, the anode was consumed before steady-state conditions were obtained. Since long warmup times were undesirable because of limitations in maximum anode length, average heat fluxes were used in this study. Except in extreme cases, all the calibration data taken lie between $\pm 10\%$ bounds about the average. Data outside these bounds have been rerun to check for operational errors. The average flux distributions obtained without a specimen dome in the system are shown in Figs. 7 and 8 for 160-amp operation in the horizontal and the vertical positions, respectively. Some of the irregular form of the flux distribution appears to

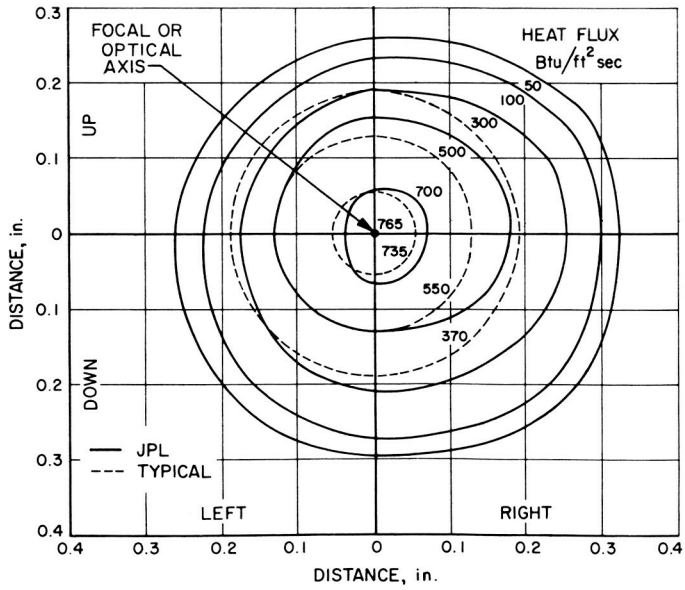

Fig. 7. Heat-flux distribution in an arc imaging furnace, horizontal position, 160-amp operation

be due to mirror imperfections which distort the image of the circular source.

The calibrated radiometer was then used to determine the distribution of the heat flux inside a specimen dome. Traverses along, or parallel to, the focal or optical axis were made by setting the radiometer sensing spot inside the dome, and ½ in. above the sealing surface of the dome. The radiometer was then shimmed down by small steps, representative of typical plastic surface recessions during exposure. The dome retained its initial set position during the shimming operation. Figure 9 shows an example of a resultant set of curves from traverses along the focal axis inside a particular specimen dome, at a 160-amp power setting. The two curves are representative of the maximum and minimum flux distributions possible from the operational drift mentioned above. Since the domes were not identical, curves of this nature were measured for each dome.

There is one inherent error in the traverses along, or parallel to, the focal axis. The calibration in the focal plane is not directly applicable to measurements along the focal axis. The calorimeter sees more of the reimaging mirror than does the radiometer. When the radiometer spot is positioned in the focal plane, the conical surface (Fig. 5) of the spot shield blocks approximately 35.5% of the total possible view angle from the mirror. When the radiometer is moved closer to the mirror, a greater view angle is blocked, whereas, when it is moved away from the mirror, the view angle gradually increases until the entire mirror is seen. (The ends of the calibration curves in Fig. 9 can be as much as 15 to 20% in error if the change in view angle is not taken into account.) This geometric problem does not affect the calibration in the focal plane, but it does require the use of a geometric correction factor along the focal axis. For short runs near the focal plane, this correction is negligible.

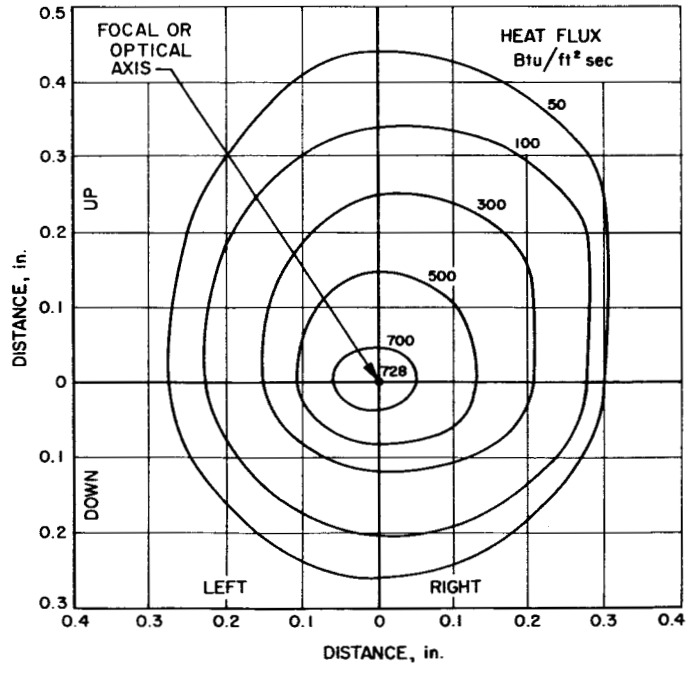

Fig. 8. Heat-flux distribution in an arc imaging furnace, vertical position, 160-amp operation

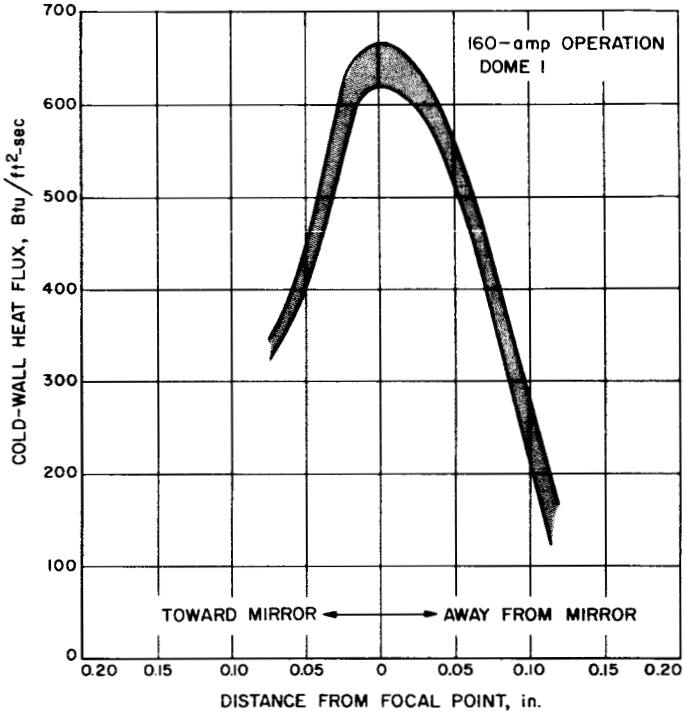

Fig. 9. Variations in the cold-wall heat flux along the focal axis

C. *Test Procedures and Evaluation of Data*

Polymeric specimens were run in the arc imaging furnace at heat fluxes of 100 to 1000 Btu/ft²-sec in vacuum and in artificial atmospheres. The test arrangement for the vacuum run is shown in Fig. 3. The specimen-holder assembly was first centered on the focal axis. A 2-in. × 2-in. × ½-in. specimen was then centered on the flat Pyrex plate of the specimen-holder assembly, and the entire assembly was moved along the focal axis until the exposed face of the specimen was located at the desired initial heat-flux position. A Pyrex vacuum dome was placed over the specimen, with the exhaust always pointing along the specimen-positioning arm. The ground-glass

flange of the dome was sealed to the flat Pyrex plate with high-temperature vacuum grease. The dome was connected to the collection system by a short plastic-tubing joint, sealed with the same high-temperature grease and protected from the radiant energy by a loose wrap of highly reflectant aluminum foil. (Long runs showed no measurable joint degradation.) The dome and one side of the collection system, including the surge volume, were pumped to a vacuum of less than 10 μ. The collection system was then sealed off from the vacuum pump. The arc was struck and was given time to stabilize. The specimen was then exposed to the radiant energy for a predetermined time period by operation of the shutter mechanism. The collection system was then sealed from the dome, and the specimen was removed for examination. Pressure changes, visual observations, and, occasionally, back-surface temperature measurements were the only data recorded during actual runs.

Runs using artificial atmospheres were only slightly different. The domes used for these runs (Fig. 4) have two openings. The larger one, the exhaust, was connected to the collection system in the same manner as for vacuum runs. The smaller opening was connected to a gas-metering system capable of providing helium, argon, lab air, nitrogen, carbon dioxide, or any combination thereof. A small baffle was placed inside the artificial-atmosphere domes just in front of the inlet to deflect the gas stream across the top of the dome. If the flow rate was kept below 3000 cc/min (STP), no blowing effect would be noted in the molten layer of the specimen, and no molten-layer splattering would reach the dome. For most of the atmospheric-pressure tests, the collection system was entirely bypassed. For reduced-pressure tests, the exhaust was run through the collection system, and a stopcock was used as a pressure-controlling, throttling device between the collection system and the vacuum pump.

Before exposure, specimens were weighed and examined visually for casting or molding imperfections. Surface variations were also noted. After exposure, the specimens were again weighed and were examined visually. Vaporization depths were measured, using a thread micrometer with a pointed head, at the focal axis and at four positions ⅛ in. from the focal axis in the transverse directions. Melt depths were also measured at the same five positions. (If melt depths were needed, specimens were cut and thicknesses were then measured directly.) If the measured vaporization depths at all five positions fell on the same straight-line curve of integrated flux vs surface recession, it was assumed that the technique was valid, and that there was no significant lateral mass flow in the melt. Intrinsic-viscosity measurements were taken on both the unmelted and the melted layers to determine any molecular-weight changes due to partial degradation in the melt.

If splatter was observed, weight-gain measurements were taken on the hemispherical vacuum domes. Where possible, the splattered materials were scraped from the dome and analyzed for molecular weight by osmometry or ebulliometry.

Most of the degradation products were condensed in the collection system. The light fraction (hydrogen, methane, etc.) was expanded into the surge volume. This fraction was then pumped out of the collection system with the Toepler pump, its volume measured (adjusting for the amount lost in the sample dome), and a sample re-collected for mass spectrographic analysis. The products condensed in the liquid nitrogen traps were fractionated by distillation techniques. Most of the time, only one fraction was collected: those gases which condensed between liquid nitrogen temperatures and room temperature. Sometimes, though, when a polymer had a large spread in the molecular weights of the degradation products, it was convenient to collect an additional fraction: those gases which condensed between carbon dioxide slush temperature and room temperature. The fractions were analyzed by gas chromatography, with identification of the unknown chromatography peaks by further fractionation and mass spectrographic analysis. Any residue remaining in the liquid nitrogen traps after fractionation was scraped out and analyzed for molecular weight by osmometry or ebulliometry.

The total heat input seen by any small unit area of interest was found by plotting against time the average heat fluxes at the initial specimen surface and at each depth after degradation and vaporization, and then graphically integrating the curve obtained for the time period represented by each run. This total heat input then represented the total radiant heat which would reach a cold black-body surface receding in the same manner. So far, no attempt has been made to measure the portion of the total heat input which was actually absorbed, rather than reflected or transmitted, at the surface of the specimens and by the evolved gases.

D. Materials Tested

The initial proof of method for the system was performed with three "commercial" polymers of a supposedly high grade. These polymers were polymethylmethacry-

late, polyethylene, and polytetrafluoroethylene. Little is known about these particular polymers concerning exact structure, additives, polymerization method, and fabrication methods and techniques. Because of this, only broad general statements can be made as to their differences or as to reasons for any observed peculiarities. Initial results on a special high-purity grade of polytetrafluoroethylene (Table 1) are also reported, for comparison.

Table 1. Presently available data on special high-purity polytetrafluoroethylene

Material designation	Teflon 7[a]
Fabrication process	Compression molded, 8,000 to 10,000 psi, in cold mold. Deaired and held at that pressure. Sintered in oven at 382°C to drive off end groups from polymerization process. When gel stage achieved, cooled to room temperature at rate of 28°C/hr.
Crystalline melting point, °C	327
Molecular weight	3 to 10 million
Refractive index	1.34
Melt viscosity, poise	
At 330°C	10^{12}
At 390°C	10^{11}
Specific gravity	2.1
Specific volume, cm^3/g	
At 15°C	$0.554 + 1.17 \times 10^{-4} T$
At 40 to 300°C	$0.454 - 1.37 \times 10^{-4} (T - T_0)$

[a]E. I. du Pont de Nemours and Co., Inc.

III. RESULTS

A. Polymethylmethacrylate

Table 2 summarizes some of the presently accepted data on the thermal stability of polymethylmethacrylate. Since this polymer degrades by unzipping fully to monomer without observable melting or swelling, it was believed that polymethylmethacrylate could best be used to prove the method outlined above. An idealized cross section of a typical polymethylmethacrylate specimen after exposure to the heat flux of the arc imaging furnace is shown in Fig. 10. Figure 11 illustrates the linear relation between the total integrated cold-wall heat flux to the receding polymer surface ($\int^t Q$ in Btu/ft^2) and the vaporized depth (VD in inches). The points represent measurements both along the focal axis and at points ⅛ in. away from the focal axis in each of four opposing directions. A least-squares fit of the points in Fig. 11 yields

$$\int^t Q = 1440 + 109{,}000\,(VD) \qquad (1)$$

where the first constant represents the average amount of heat absorbed per unit area before vaporization begins, and the second constant is an "effective heat of vaporization."

Figure 12 shows the linearity of the relation between the average cold-wall heating rate and the vaporization rate. The values were taken from an averaging of the two heat-flux curves of Fig. 9 after an adjustment had been made for the time up to the start of vaporization or degradation.

A number of restrictions must be realized in any consideration of the linearity noted above. The total integrated cold-wall heat flux quoted is that which would be

Table 2. Thermal-stability data for polymethylmethacrylate

Property	Value	Reference
Degradation temperature, °C	330	5
Ceiling temperature, °C	220	5
Activation energy, kcal/mol		
Low molecular weight[a]	28 to 32	6, 7, 8
High molecular weight[b]	40 to 55	6, 7, 8
Mode of degradation		
Low molecular weight[a]	Reverse polymerization	6, 7, 8
High molecular weight[b]	Reverse polymerization	6, 7
Monomer in degradation product, %		
Low molecular weight[a]		
At 500°C	96	9, 10
At 800°C	82	10
At 1200°C	12	10
High molecular weight[b]		
At 500°C	100	9
Density, g/cm^3		
At 21°C	1.19	11
Specific heat, cal/g-°C		11
At 21°C (T_0)	0.310	
Temperature dependence	$0.310 + 0.00151\,(T - T_0)$	
Thermal conductivity, cal/sec-cm^2-°C/cm		11
At 21°C (T_0)	0.000365	
Temperature dependence	$3.65 \times 10^{-4} + 1.80 \times 10^{-7}\,(T - T_0)$	

[a]Approximately 150,000.
[b]Approximately 5,000,000.

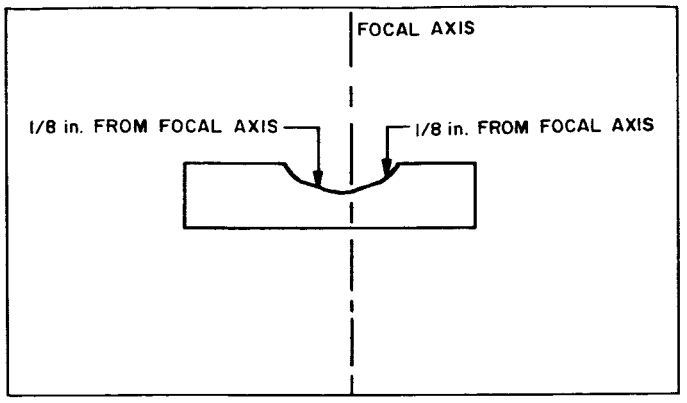

Fig. 10. Idealized cross section of a polymethylmethacrylate specimen after exposure in an arc imaging furnace

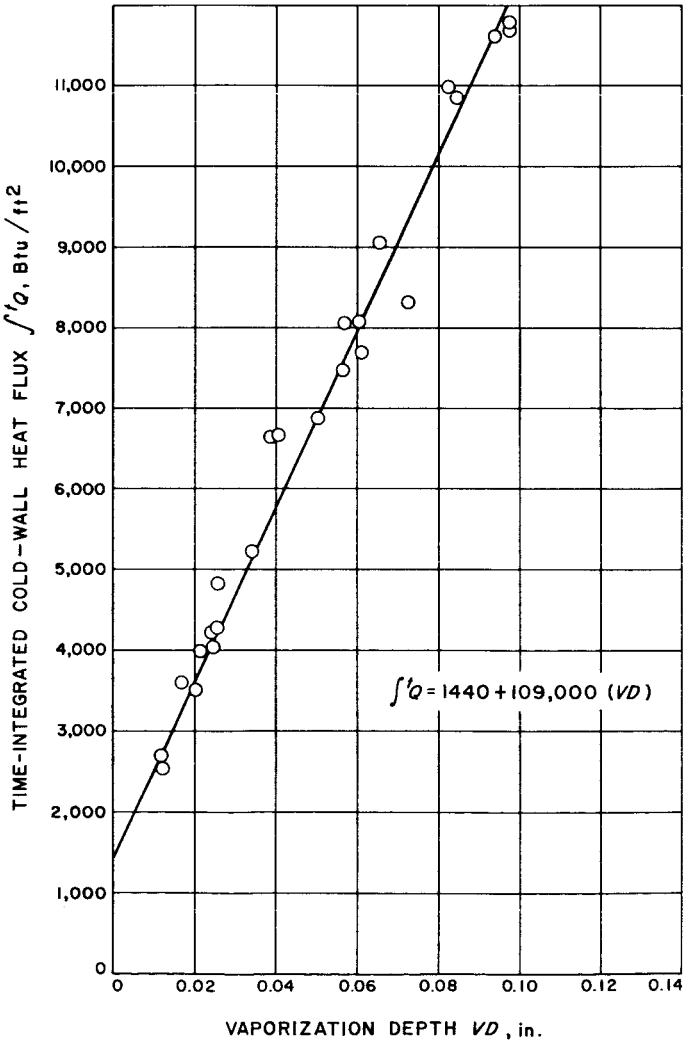

Fig. 11. Effect of total radiant-energy input on the thermal degradation of polymethylmethacrylate in a vacuum

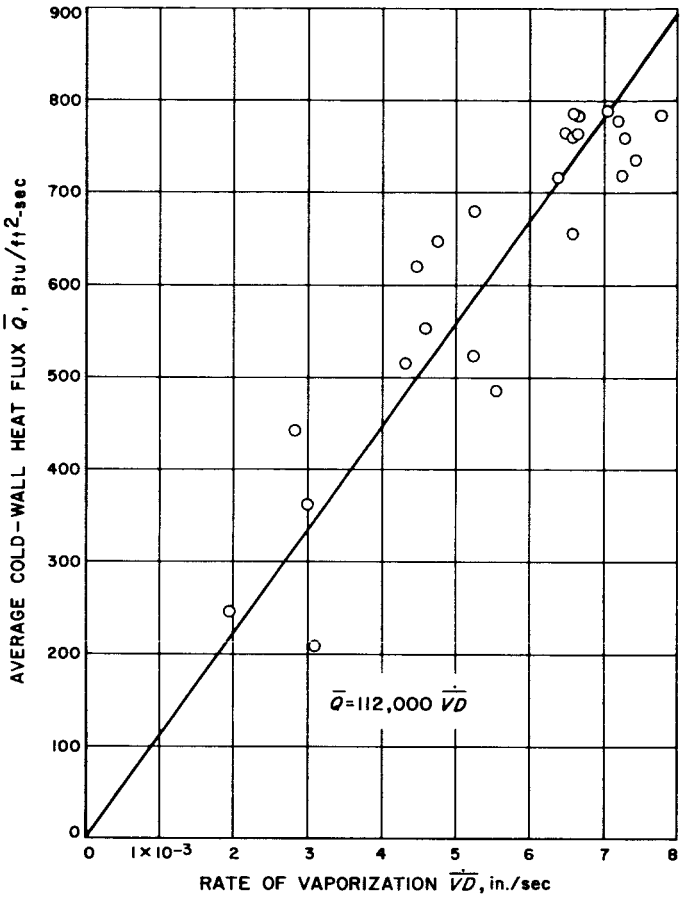

Fig. 12. Effect of average heat flux on the rate of thermal degradation of polymethylmethacrylate in a vacuum

transferred to a body at near room temperature and with approximately 98% absorptivity at the surface. The surface of unroughened polymethylmethacrylate will reflect about 4% of the total visual-range energy directed perpendicularly to it and will reflect greater or lesser amounts as the wavelength varies. Since the reflectance increases as the angle of incidence varies farther from the perpendicular, an ellipsoidal system like the arc imaging furnace will lose a significant amount of the total energy impinging on the sample surface. Of the energy which is not reflected away, about 96% of that in the visual range will be transmitted through a ½-in. sample without absorption. Therefore, the first constant in Eq. 1 is a function of the surface absorptivity and reflectivity, as well as the density, specific heat, and thermal conductivity normally considered in simple heat-conduction problems. (In this study, the polymethylmethacrylate surface was roughened to produce an initial opacity of approximately 90%.) The second constant, on the other hand, is less dependent on transmission prop-

erties, since this polymer becomes more opaque at the surface as soon as vaporization begins. The second constant is also dependent upon any blocking effect due to heat absorption by the vaporizing species, as well as any "real" heat of vaporization or heat of degradation.

This behavior is demonstrated in Fig. 13, which shows a typical recorded trace of the temperature of a chromel-alumel thermocouple at the back surface of a roughened polymethylmethacrylate specimen. The thermocouple was first heated by transmitted energy. At the start of degradation, the specimen became opaque to the energy, and the thermocouple cooled off by conduction through the specimen and the supporting Pyrex plate until additional heat was transferred to it by conduction from the hot specimen surface.

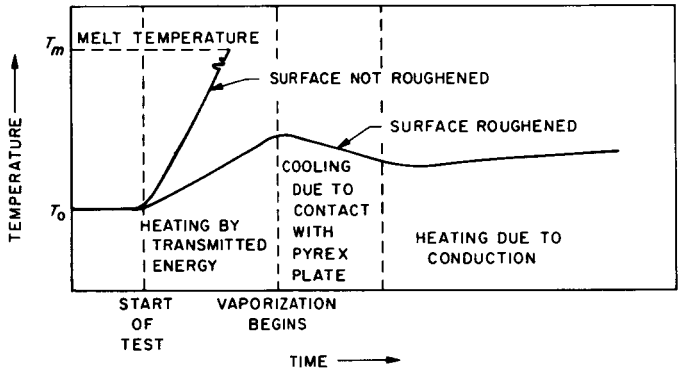

Fig. 13. Idealized temperature record for a chromel-alumel thermocouple at the back surface of polymethylmethacrylate

The products of degradation were collected and run through gas chromatography. Only one readable peak was found from the gas chromatography, regardless of the heating rate used during a test. This peak was identified as methylmethacrylate monomer by mass spectrographic techniques. The mass spectrometer also showed traces of some unidentifiable organic or organics with larger mass numbers. It is of interest, at this point, to compare the results quoted in Table 2 from work by Madorsky and Straus at NBS (Refs. 9 and 10) with those obtained at JPL. The limited information available on the polymethylmethacrylate used in the JPL study indicates that the samples were probably of a low molecular weight. The three temperatures to which the specimens of Madorsky and Straus were heated are indicative of heating rates, rather than equilibrium specimen temperatures. It is unlikely that a material with a degradation temperature of 330°C will superheat to 1200°C. The arc imaging furnace used to heat the JPL specimens is capable of heating black-body specimens to temperatures in excess of 3000°C. Allowance for the transmission and reflection differences between a black-body and the polymeric specimens used in the present study still place results in the JPL experiment at the high end of the Madorsky and Straus series of temperatures. Thus, the 98% (or greater) monomer yield measured at JPL differs considerably from the 12% yield at 1200°C measured by Madorsky and Straus. This would seem to indicate that the way in which heat is added is much more important than the rate at which it is added.

Since the degradation products found by Madorsky and Straus at the higher heating rates were primarily products of the breakdown of monomer units, perhaps much of the additional breakdown was due to a catalytic effect of the hot Pyrex jacket (~1200°C) surrounding the specimens in the NBS apparatus. The domes used in the JPL apparatus reached a peak temperature of 300°C during only the longest runs. A further study of this effect has been made, using a thin slab of pyrolytic graphite supported with fused silica rods at a distance between ⅛ and ¼ in. above a specimen of polymethylmethacrylate (Ref. 12). The surface temperature of the pyrolytic graphite face on the side toward the specimen was heated to 1500°C. All this was carried out inside a standard 4-in.-diameter vacuum dome, and the products of degradation from the polymethylmethacrylate, radiantly heated by this 1500°C surface, were collected and analyzed. The products were again identified as better than 98% monomer. The absence of large fractions with lower molecular weights, representative of the monomer breakdown observed by Madorsky and Straus (Ref. 10), would again seem to indicate that a difference occurs in the degradation mechanism when a specimen is heated from all sides and when it is heated from one side only. The degradation-product yields of the Madorsky and Straus experiment also showed an oxygen content in the form of carbon monoxide and carbon dioxide far above that obtainable from the polymer itself or from any absorbed oxygen or water. Perhaps, then, the hot oxide surface of the surrounding Pyrex in the NBS apparatus caused an oxidation of the monomeric units which did not take place on the reducing surfaces of the pyrolytic graphite used in the JPL apparatus.

B. Polytetrafluoroethylene

Table 3 summarizes some of the presently accepted data on the thermal stability of polytetrafluoroethylene. There is some difference of opinion on the exact mecha-

Table 3. Thermal-stability data for polytetrafluoroethylene

Property	Value	Reference
Degradation temperature, °C	510	5
Ceiling temperature, °C	580	5
	608	13
	712	14
Melt temperature, °C	327	15
Activation energy, kcal/mol	80.5	16
	83	13
Mode of degradation	Terminal initiation with complete depropagation	13, 16
Monomer in degradation product, %		
500°C	95	10
510°C	94–97	13
800°C	91	10
1200°C	78	10
Density, g/cm^3		
25 to 325°C	$2.33 - 7.64 \times 10^{-4} (T - 25°C)$	17
325 to 450°C	$1.919 - 1.16 \times 10^{-3} (T - 325°C)$	17
Specific heat, cal/g - °C		
Powder, 0 to 327°C	$0.223 + 2.50 \times 10^{-4} T$	18
Drawn (crystalline), 0 to 327°C	$0.223 + 2.39 \times 10^{-4} T$	18
Thermal conductivity, cal/cm^2-sec		Extrapolated from data of 19
$T_0 = 25°C$	$5.8 \times 10^{-4} + 8.50 \times 10^{-7} (T - T_0)$	

nism by which polytetrafluoroethylene initiates depolymerization, but degradation products are usually 95–99% monomer, pointing to an unzipping mechanism somewhat similar to that for polymethylmethacrylate. Two grades of polytetrafluoroethylene were used in this study, a special high-purity grade and a "commercial" grade.

The high-purity polytetrafluoroethylene showed a linearity in the relationship between the total integrated cold-wall heat flux and the vaporization depth, but only with points along the focal axis and only on runs beginning with the same initial-surface position. Figure 14 shows the data for three different initial-surface positions. The points obtained when the initial surface was located at the focal plane may be represented by a least-squares straight line,

$$\int^t Q = 1700 + 336{,}000\,(VD) \qquad (2)$$

and those points obtained when the initial surface was 0.05 in. behind the focal plane by

$$\int^t Q = 1790 + 278{,}000\,(VD) \qquad (3)$$

Much of this variation with initial-surface position and with lateral distance away from the focal axis was caused by an increase in the lateral flow of heat within the specimens, which was due to a combination of the increasing transparency of polytetrafluoroethylene with temperature and the oblique angles with which much of the energy from the ellipsoidal focusing system impinged on the specimen surface. The reflectivity of the high-purity-grade material was measured to be less than 0.1% in the visual range.

Figure 15 shows an idealized drawing of a typical temperature history taken on a thermocouple at the back surface of high-purity polytetrafluoroethylene. At the start of the exposure period, the thermocouple appeared to be heated by the transmitted component of the energy. This thermocouple temperature leveled out until vaporization began. At this point, the temperature began increasing again as the decrease in effective thickness increased the transmission. Finally, the rate at which the temperature was rising further increased because of conductive heating.

The "commercial"-grade polytetrafluoroethylene also showed a linear relationship between the total cold-wall

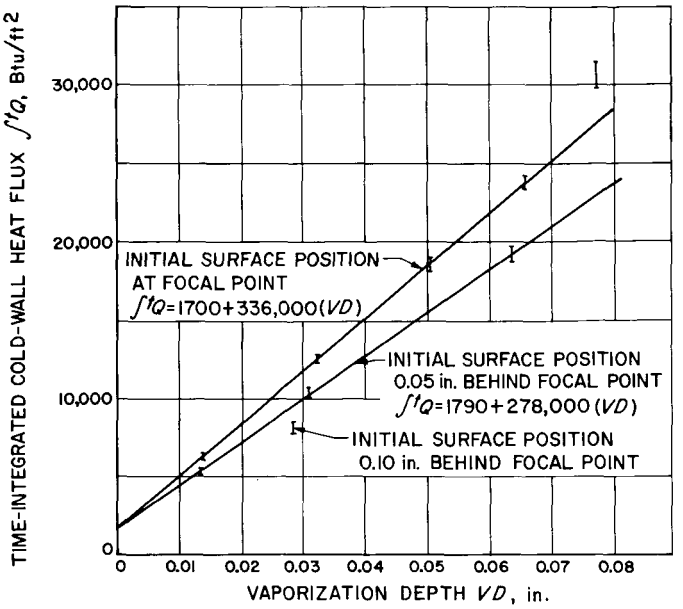

Fig. 14. Effect of total radiant-energy input on the thermal degradation of polytetrafluoroethylene (high-purity grade) in a vacuum

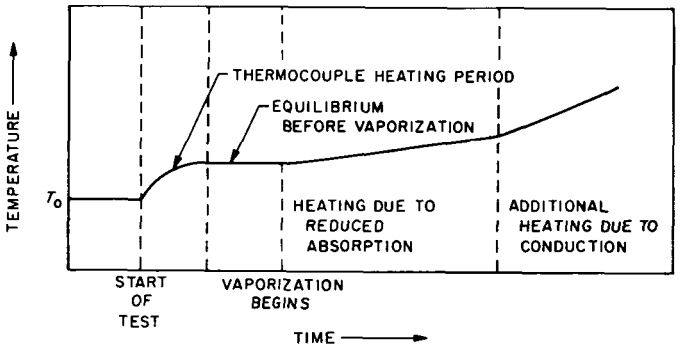

Fig. 15. Idealized temperature record for a chromel-alumel thermocouple at the back surface of polytetrafluoroethylene

heat flux and the vaporization depth (Fig. 16), but, for this material, the slope did not change with change in initial-surface position. On the other hand, many of the samples tested showed a discontinuity similar to that shown by the higher curve in Fig. 16. This discontinuity was apparently due to a molding imperfection in the second group of samples at approximately 0.02 in. below the surface. This imperfection could be detected visually and remained at a constant depth parallel to the exposed surface for all of the second group of samples. Figure 17 shows an idealized cross section of a typical "commercial" polytetrafluoroethylene specimen before and after the vaporization depth had reached the imperfection level.

The imperfection apparently caused a reflection of the heat energy outward from the focal axis, enlarging the diameter of the vaporized area. Visually, the polymer appeared to "flow" towards the focal axis, and a hump of waxy material was noted at the focal axis after long exposures. Similar effects were also observed in other specimens at other depths and, in some cases, at more than one depth. In each case, the depth at which this lateral effect took place was coincident with a visually noted plane of imperfection. A least-squares fit of the

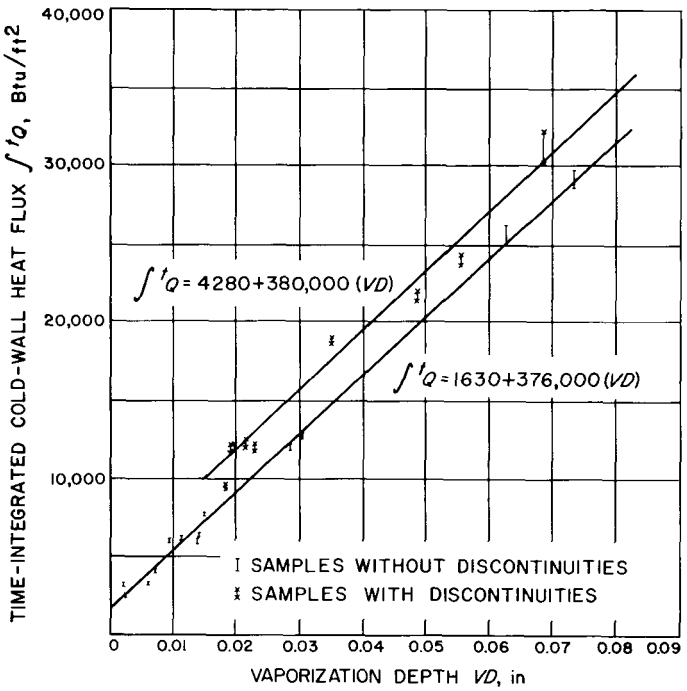

Fig. 16. Effect of total radiant-energy input on the thermal degradation of polytetrafluoroethylene ("commercial" grade) in a vacuum

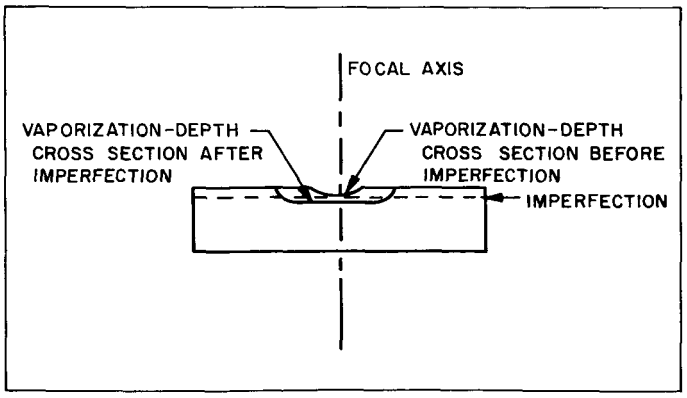

Fig. 17. Idealized cross section of a polytetrafluoroethylene specimen after exposure in an arc imaging furnace

points from the specimens without imperfection planes yields the expression

$$\int^t Q = 1630 + 376{,}000\,(VD) \qquad (4)$$

A least-squares fit of the second group of points gives a similar slope, but, in this particular case, it is probably a coincidence. Since the average rate at which the heat flux was added was different in several of the runs, the delay time, due to the observed lateral effect, was also different. This delay difference should vary the magnitude of the shift in the curve.

Several related oddities were noticed in the "commercial"-grade polytetrafluoroethylene. If three supposedly identical samples from adjacent locations on the same sheet were run under identical conditions, one usually had a noticeable "melt," or waxy layer, which was absent in the other two, despite the fact that all three had nearly identical vaporization depths. Of the three specimens, one might show a noticeable splatter on the dome. The one which showed this effect would be only at random the same specimen as the one showing the waxy or "melt"-layer effect. One large "commercial"-grade slab, supposedly of a purer grade than the standard "commercial" materials used for the data in this study, did not show the molding imperfections observable in the recorded samples, but was so filled with carbonaceous inclusions that about half of the samples burst and burned during testing, splattering large pieces of sample about the dome and covering the inside of the dome with black soot.

The degradation products from polytetrafluoroethylene were collected and analyzed on the mass spectrometer. The products were identified as primarily monomer, but some unsaturated C_3, C_4, and C_5 fluorocarbons were also present, a result similar to that reported by Madorsky and Straus (Ref. 10). Preliminary quantitative identification from gas chromatography fractionation is shown in Table 4. There is some doubt about these values, since a liquid fraction became observable with time, indicating some repolymerization of the material. However, the reported values are indicative that the trend toward a lower per cent of monomer with increased furnace temperature observed by Madorsky and Straus might be due to the hot surface of the Pyrex container or to some other effect of the method of heating, rather than to any heating-rate effect.

Table 4. Degradation products of polytetrafluoroethylene

Species identified	Average of values from Ref. 10, %			JPL study
	500°C	800°C	1200°C	>1200°C
H_2	—	—	—	—
HF	0	0	0.3	0
CF_4	1.3	1.7	2.2	0
C_2F_4	95.0	91.2	78.1	98.8
C_3F_6	3.7	6.2	5.5	1.2
Solid products	0	0.9	13.9	?

C. *Polyethylene*

Table 5 summarizes some of the presently accepted data on the thermal stability of polyethylene. For the purposes of this experiment, polyethylene varies in four important ways from the polymethylmethacrylate and the polytetrafluoroethylene discussed above:

1. The material degrades by random scission rather than by unzipping.
2. The thermal conductivity decreases, rather than increases, when the temperature rises above room temperature.
3. There is a large spread between the melt and the degradation temperature.
4. A significant density change takes place upon melting.

The average thickness expansion due to loss of crystallinity was roughly measured as 9% for the polyethylene used in this experiment. The expanded melt layer may best be illustrated by the idealized cross section shown in Fig. 18.

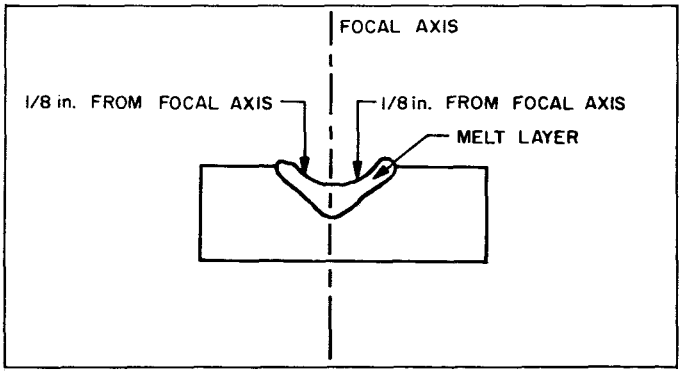

Fig. 18. Idealized cross section of a polyethylene specimen after exposure in an arc imaging furnace

Table 5. Thermal-stability data for polyethylene

Property	Value	Reference
Melt temperature, °C	137	15
Degradation temperature, °C	400	5
Ceiling temperature, °C	400	5
Activation energy, kcal/mol	60–70	20
	66	21
	68	22
Mode of degradation	Random scission	5, 20, 21, 22, 23
Monomer in degradation product, %		
500°C	0	10
800°C	5.4	10
1200°C	22.3	10
Density, g/cc		
21°C	0.9–1.0	24
>21°C	Dependent on branching but decreases significantly	24
Specific heat, cal/g-°C		
Crystalline form	$0.41 + 0.0021\ T$	25
Liquid form	$0.50 + 0.0011\ T$	25
Thermal conductivity, cal/cm²-sec-°C/cm		
$T_0 = 21$°C	0.000841	11
Temperature dependence, cal/cm²-sec-°C/cm	$8.41 \times 10^{-4} - 2.37 \times 10^{-6}\ (T - T_0)$	11

The effect of total integrated cold-wall heat flux on the thermal degradation of polyethylene in a vacuum is shown in Fig. 19. The curvature seen above 0.07 in. in vaporization depth was due to splattering of the polyethylene onto the Pyrex vacuum dome. This splattering was caused by the evolution of low-molecular-weight gases within the melt layer. Of the material lost during arc-imaging-furnace exposure in a vacuum, 85% was splattered onto the Pyrex vacuum dome. Only 4% was collected as gas, and the remaining 11% was collected as solid residue in the liquid nitrogen traps and throughout the glass connections between the dome and the traps. By measuring the heat-flux distribution under the splattered domes after each exposure, a new total heat-flux variation with time can be determined. If these new heat-flux values had been used to determine the total integrated cold-wall heat flux for those points above 0.07 in. in vaporization depth, all the points would have been within 10% of the least-squares straight line determined from those runs with less than 0.07 in. in vaporization depth. Since measurements of dome weight gain showed insignificant splatter or none below the 0.07-in. vaporization depth, it was believed that the following equation, obtained from a least-squares fit of these shorter-time data points, was valid for this system:

$$\int^t Q = 400 + 47{,}000\ (VD) \qquad (5)$$

All the data were corrected for expansion from the crystalline to the amorphous state by adding 9% of the melt depth to the measured vaporization depth. The validity of this correction was proven by the fact that the curve (Fig. 20) for the average cold-wall heat flux ($\bar{Q}$, Btu/ft²-sec) vs the rate of vaporization ($\overline{VD}$, in./sec) could not be fitted to a straight line until the melt expansion correction was added to the values. This meant that points with the same total flux but different average fluxes would not appear as coincident in Fig. 19 until the melt expansion correction was added. It was also important that, despite this significant expansion, all points on the curves fitted, regardless of whether they were taken on the focal axis or at a position ⅛ in. away from the focal axis (Fig. 18). Apparently, none of the melt reached a viscosity during the time of operation sufficiently low to cause significant flow of the polyethylene by gravity from the sides of the vaporized area to the center of that region. The melt depth (Fig. 21) also showed a linearity in the low total-heat-flux region similar to that in Fig. 19. The least-squares curve representing the melt depth (MD) is

$$\int' Q = 16{,}080\,(MD) \qquad (6)$$

Reflection and transmission of the heat energy must also be considered in analyzing polyethylene. The reflectivity of this polyethylene was measured as about 1%, and the room-temperature transmission through a ½-in. specimen varied from specimen to specimen between 5 and 20%. A thermocouple at the back surface of the specimens showed a rapid rise in temperature, due to transmission, during the first 20 to 30 sec. After 20 or 30 sec, depending on the average heating rate, the rate of temperature rise in the thermocouple increased by an order of magnitude or more. This may be explained by the visual observation that polyethylene becomes extremely transparent at some temperature below the temperature of transition from the crystalline to the amorphous state. In the present experiment, the boundary of the transparent portion reached the rear of the ½-in. specimen even before the melt boundary. This author has found a dearth of data on the change in optical properties of polyethylene with temperature.

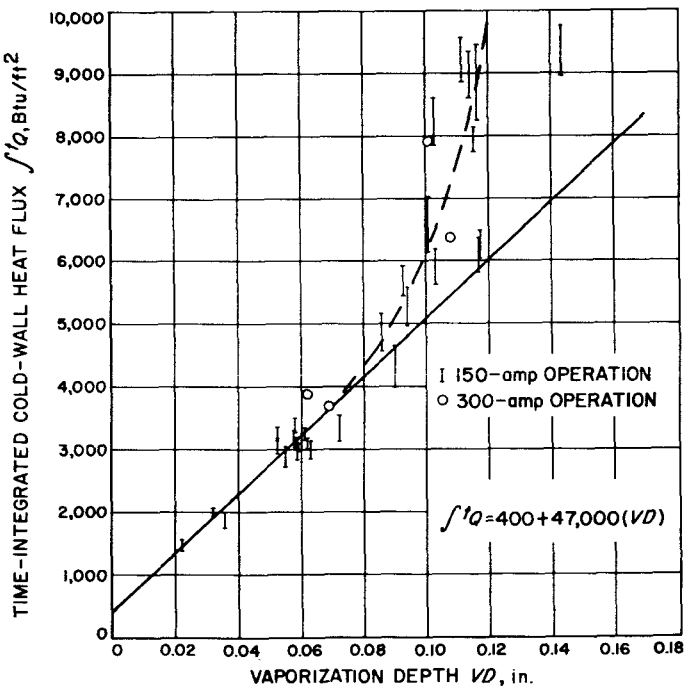

Fig. 19. Effect of total radiant-energy input on the thermal degradation of polyethylene in a vacuum

The volatile portion of the degradation product was collected and analyzed through gas chromatography, with peak identification by fractionation and mass spectroscopy. An approximate distribution of volatile products by weight for both a normal test and a test using hot pyrolytic graphite as a reradiator is shown in Table 6,

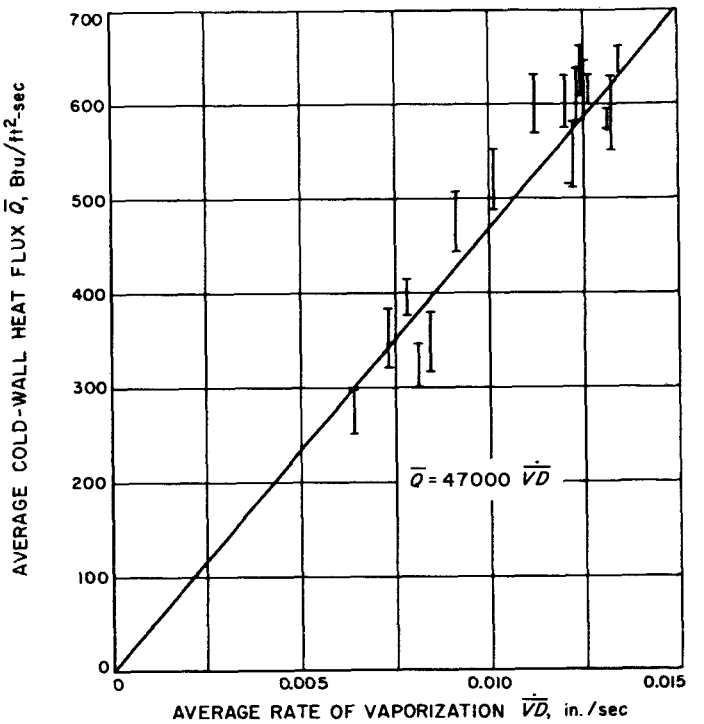

Fig. 20. Effect of average radiant-heat flux on the thermal degradation of polyethylene in a vacuum

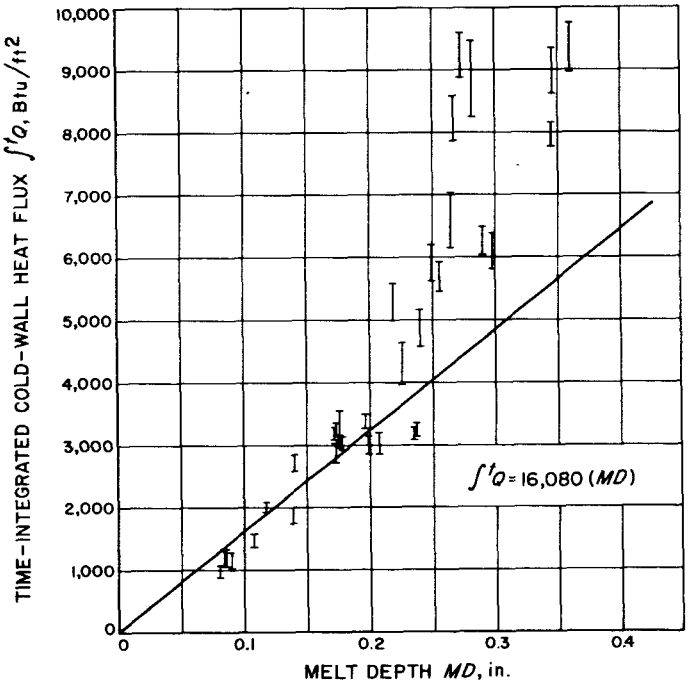

Fig. 21. Effect of total radiant-energy input on the melt depth of polyethylene in a vacuum

Table 6. Comparative distributions of species identified in polyethylene and polymethylene degradation products which were volatile at room temperature

Species identified	Distribution of species in degradation products, %					
	Polyethylene[a]				Polymethylene[a]	
	JPL study		Ref. 26	Ref. 10	Ref. 10	Ref. 10
	Heating rate = 160 cal/cm^2-sec	Wall temperature under pyrolytic graphite = 1500°C	Furnace temperature = 405°C	Furnace temperature = 500°C	Furnace temperature = 800°C	Furnace temperature = 1200°C
C_2H_2	5.8	3.2	—	—	—	6.1
C_2H_4	67.5	62.7	4.8	—	24.6	46.8
C_2H_6	—	—	14.3	1.7	1.4	1.7
C_3H_4	0.9	1.3	1.2	1.7	0.9	4.4
C_3H_6	15.8	13.1	—	1.7	12.7	13.4
C_3H_8	3.3	4.1	15.3	3.4	—	0.8
C_4H_6	1.8	4.4	—	5.1	4.1	11.3
C_4H_8	3.7	8.2	24.5	5.1	17.7	5.8
C_4H_{10}	0.6	1.3	16.8	1.7	1.8	—
C_5H_8	0.6	1.7	8.3	13.6	9.6	—
C_6H_{10}	—	—	6.8	—	—	—
Larger molecules	—	—	Traces	Traces	—	Traces
	Percent of product (collected in liquid nitrogen trap) which is gaseous at room temperature					
	26.7%	—	23.1%	5.9%	22.0%	47.7%

[a]In vacuum.

together with comparative data from the literature. No conclusions can be drawn from the runs made under normal operation, since the loss mechanism was dominated by splattering, and the volatile portion included only 4% by weight of the total material lost. Preliminary measurements for this run on the molecular weight of the residue in the liquid nitrogen trap and the splatter on the dome have indicated a similarity in the two products, with the molecular weights of both samples considerably below the value of 692 quoted by Madorsky, et al (Ref. 26). The run using the flux reradiator had test conditions more similar to those used by Madorsky and Straus, and the data fit very well into the progression set up by the temperatures of their three furnaces. A very light volatile fraction containing hydrogen and methane was collected from the diffuser run, but was not observed in runs without the diffuser. The increasing percentage of monomer with rising wall temperatures was expected from the hypothesis of Oakes and Richards (Ref. 20) that increases in temperature or heating rate produce a higher rate of C-C bond breakage in an equivalent mass or volume. How much of the increase in lighter products was due to increases in heating rate and how much was due to additional breakdown resulting from contact with the hot surface is unknown.

Polyethylene was also tested in artificial atmospheres. The effect of the total radiant-energy input on the thermal degradation of polyethylene in helium at atmospheric pressure is plotted in Fig. 22. The curve is a straight line throughout the heat-flux range. The helium deflected across the top of the dome by the baffle in the gas inlet line swept the splatter out without allowing it to stick to the dome. Even so, the residue collected in the liquid nitrogen traps and in the lines between the dome and the traps did not account for the 96% splatter and residue obtained in the vacuum runs. The volatile fraction was much larger than that recorded in vacuum

operation, and a greater per cent of higher-molecular-weight species appeared in the volatile fraction. A least-squares fit of the curve in Fig. 22 is

$$\int^t Q = 360 + 73{,}000\,(VD) \qquad (7)$$

It is interesting to note that the first constant is similar to the value of 400 calculated for the vacuum runs, but that the second constant is considerably higher. The higher second constant could be due to blocking of the radiant energy by the injected gas, or to cooling of the specimen surface by the injected gas, or to some pressure effect.

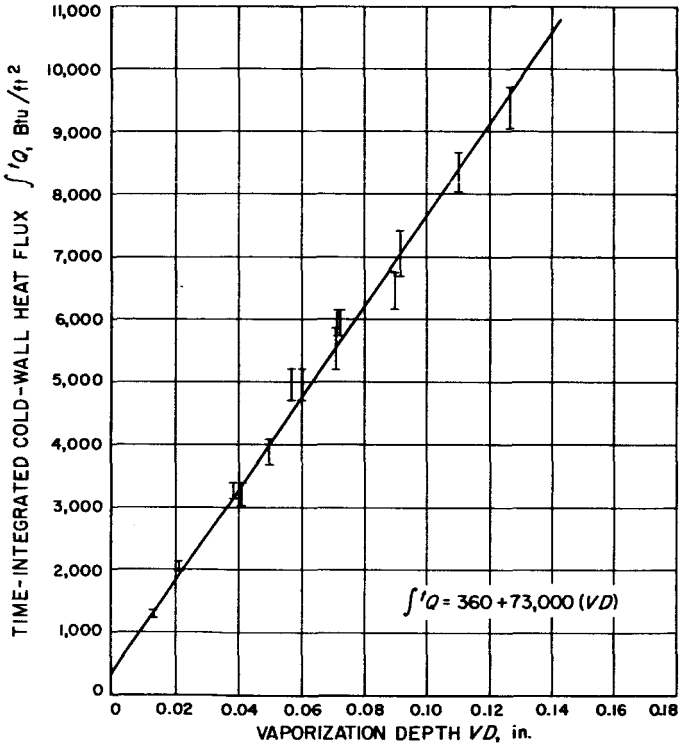

Fig. 22. Effect of total radiant-energy input on the thermal degradation of polyethylene in helium at atmospheric pressure

To check the pressure effect, a number of specimens were run for 5 sec each in identical initial positions, but with various pressures between a nominal 0 and 1 atm (absolute). For all runs, the total integrated flux was 3000–3300 Btu/ft²-sec, and the helium flow rate was held at 2800 cc/min (STP). Figure 23 shows a curve of vaporization depth vs the pressure in the dome. The depth decreased with increasing pressure to a minimum at −3 in. Hg. Numerous runs were made at pressures of −3, −2, and −1 in. Hg (gauge) without variation in the result. Runs made at atmospheric pressure, but with the degradation products removed in the liquid nitrogen traps, showed a drop to the extended curve from the lower-pressure runs. Runs made directly to the atmosphere, as in Fig. 22, showed a rise in vaporization depth for the same helium flow rates and total integrated cold-wall heat flux.

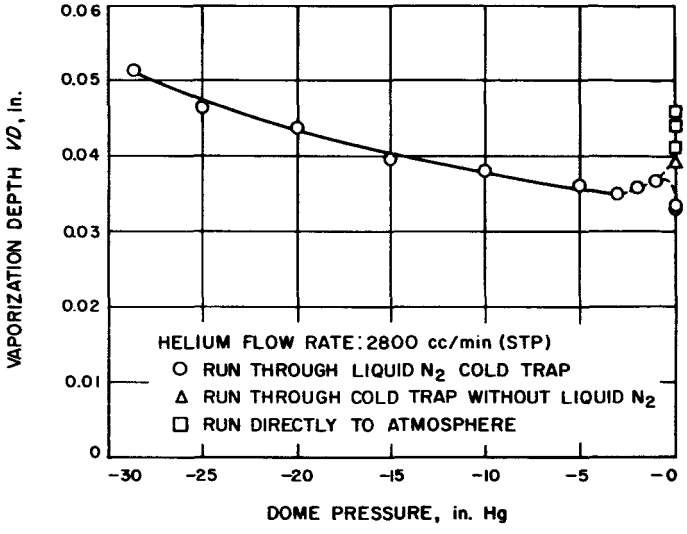

Fig. 23. Effect of reduced pressure on the thermal degradation of polyethylene with constant helium flow rate over the surface

In checking the vaporization-depth data at the lowest obtainable pressures, an interesting sidelight was discovered. Consistent differences in vaporization depths were observed for runs of identical durations without helium flow during the run, but with slight variations in the pumpdown procedures. Specimens run after being pumped down directly from air showed consistently higher vaporization depths than those in which the dome was blown out with helium for 5 min before sealing the helium from the system and pumping down. Apparently, oxygen absorbed on the surface of the dome and the specimen catalyzes the vaporization or degradation process.

To check the flow effect, several specimens were run for 5-sec intervals at atmospheric pressure, but with various helium flow rates. A curve of these data is shown in Fig. 24. No flow-rate effect is apparent in the region tested. At flow rates above 3000 cc/min, "blowing" was observed on the melt layer of the specimen. At flow rates below about 500 cc/min, splatter occurred.

The effect of different atmospheres is shown in Fig. 25. The differences are probably due to variations in radiant-

Table 7. Least-squares curves for the total time-integrated radiant energy "absorbed" by polyethylene in various artificial atmospheres

Atmosphere	Pressure	$\int^t Q = C_1 + C_2(VD)$	
		C_1, Btu/ft^2	C_2, Btu/ft^2-in.
Helium	1 atm	360	73,000
Argon	1 atm	360	68,900
Carbon dioxide	1 atm	360	62,400
Lab air	1 atm	360	62,300
Nitrogen	1 atm	360	57,300
Vacuum	10 μ	400	47,000

Note:
$\int^t Q$ = time-integrated cold-wall heat flux
VD = vaporization depth

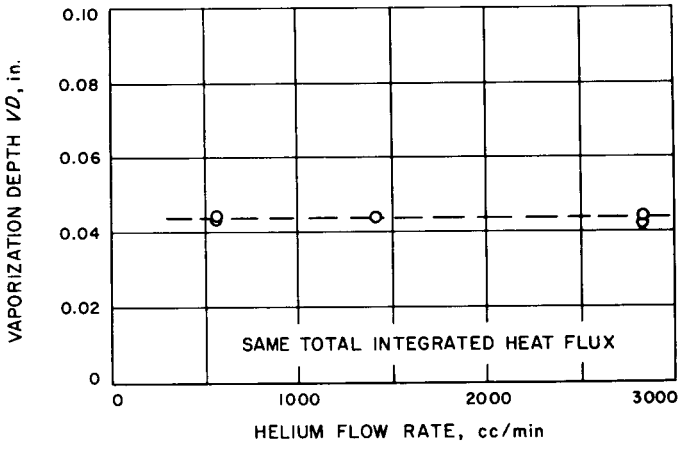

Fig. 24. Effect of helium flow rate on the thermal degradation of polyethylene at atmospheric pressure

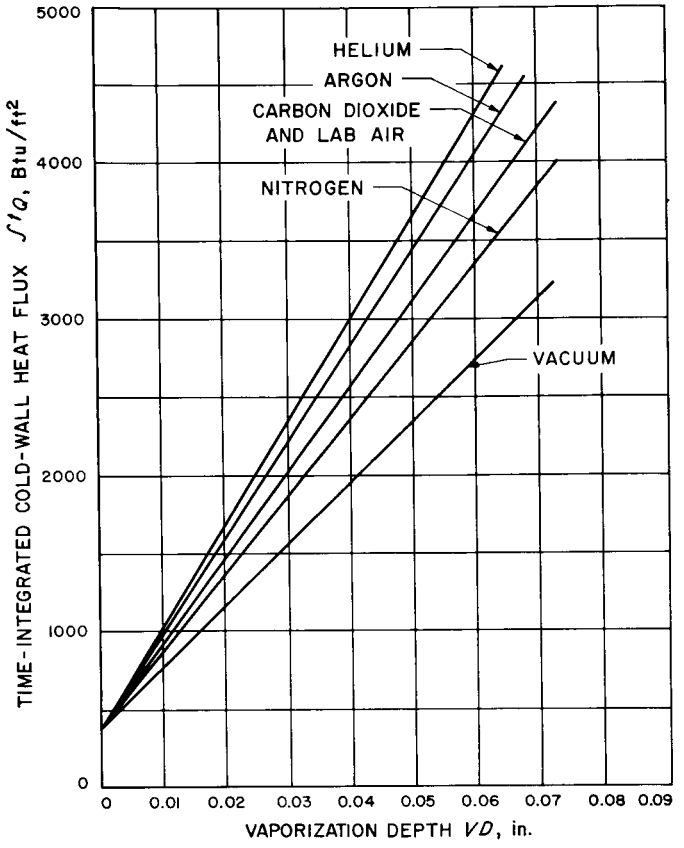

Fig. 25. Effect of total radiant-energy input on the thermal degradation of polyethylene at atmospheric pressure in various controlled atmospheres

energy absorption and chemical activity, and also to the change in the convective-heat-transfer coefficient from one gas to another. The lab air and the carbon dioxide curves were indistinguishable and are represented by one line. The curve for the vacuum operation is shown for comparison. The least-squares fits to the various curves are listed in Table 7.

IV. GENERAL DISCUSSION

Without detailed measurements of reflectivity and absorptivity, there can be no exact evaluation of the radiant-heat-absorption capacity of homogeneous thermoplastic materials in the solid or liquid state. This is especially true in this study, where the source gives off energy in a wide range of wavelengths, and where the ellipsoidal mirrors provide angles of incidence between the flat specimens and the heat energy which differ considerably from the 90-deg optimum. Therefore, the curves of linear heat input vs surface recession given in this study show only that the optical properties for each material are constant within each of the phases studied. The results also show that materials like polyethylene, with transparent melt layers, will never realize their full ablation and insulation capacity. The transparency of the melt layer causes the melt boundary to proceed much faster than the vaporizing boundary. This allows excessive heat flow to the back surface of the materials and results in splattering of undegraded, or partially degraded, material due to the evolution of low-molecular-weight gas in the melt layer.

Table 8 presents a comparative listing of "effective radiant-heat absorption capacities" calculated from the data of this study. Effective heat-absorption capacity is commonly used to estimate the relative stability or heat-protection capability of ablative materials. It is interesting to note that polyethylene, which is normally considered more stable than polymethylmethacrylate, did not show greater stability in this investigation, probably because of the large splatter loss due to transmitted energy. Polytetrafluoroethylene appears to be the best of the materials studied, with the high-purity, more homogeneous material showing a significant increase in "effective radiant-heat absorption capacity" over the "commercial" variety.

Comparison of the degradation-product data of this study with that of the literature (Tables 2, 4, and 6) shows a considerable discrepancy. In all cases, the heating rates used in this experiment were higher than those reported in the literature. For the unzipping materials, polymethylmethacrylate and polytetrafluoroethylene, the literature studies show an additional breakdown of monomeric units to lower-molecular-weight gases not seen in the JPL study. For the random-scission material, polyethylene, the JPL data fit into the reported progression of higher monomer yield with higher furnace temperatures (higher heat fluxes).

Table 8. Comparison of measured effective radiant-heat absorption capabilities of homogeneous polymeric materials

Material	Pressure	Effective radiant-heat absorption capability, Btu/lb
Polytetrafluoroethylene, special high-purity grade	10 μ	34,400
Polytetrafluoroethylene	10 μ	26,900
Polymethylmethacrylate	10 μ	17,500
Polyethylene	10 μ	9,000
Polyethylene	1 atm in helium	14,000

Fabrication techniques seem to have a major effect on the heat-absorption capabilities of homogeneous polymeric materials. The presence of inclusions of various sizes was noted in all the materials tested, regardless of any prior guarantee of purity. Generally, poor fabrication practices throughout the polymer industry add lint, grease, molding additives, and general sludge to any initially pure raw material.

Future extensions of this investigation must thus emphasize increased purity and homogeneity in fabricated specimens, as well as comprehensive measurements of the optical properties of the specimens. With this information, it is hoped that these preliminary results will become more meaningful, and that a more comprehensive mathematical model of the system may be realizable.

V. CONCLUSIONS

In summary, the conclusions resulting from the present investigation may be stated as follows:

1. A technique was developed to measure the radiant-heat absorption capabilities of polymeric materials. The technique provides reproducible data and linear curves of heat input vs surface recession which are not inconsistent with theory.
2. Comprehensive reflectivity and transmissivity measurements on polymers are necessary before a detailed analysis of the data would be meaningful.
3. The composition of the collected degradation products for polymethylmethacrylate and polytetrafluoroethylene does not agree with that reported in the literature.

ACKNOWLEDGMENTS

The author wishes to thank Thomas M. Baugh and Thomas E. Patrick, who carried out the experimental portion of this work, and Dr. Leonard D. Jaffe and Howard E. Martens for their many valuable contributions to the formulation of the experimental technique and the analysis of the final results.

REFERENCES

1. Schwartz, H. S., "New Materials and Physical Constructions for Ablative Use," paper presented at *International Symposium on High Temperature Technology*, Asilomar, California, September 8–11, 1963.

2. Pugmire, T. K., *Experimental Planetary Entry Research for Mars and Venus—1962*, Report No. R62SD84, Missile and Space Division, General Electric Company, Philadelphia, October 1962.

3. Robbins, D. L., and Kremith, R. D., *Thermal Erosion of Ablative Materials*, ASD-TDR-63-254, Aeronautical Systems Division, Wright-Patterson AFB, Ohio, March 1963.

4. Friedman, H. L., *The Pyrolysis of Plastics in a High Vacuum Arc Image Furnace*, Report No. R60SD380, Missile and Space Division, General Electric Company, Philadelphia, May 1960.

5. Wall, L. A., "Polymer Decomposition: Thermodynamics, Mechanisms, and Energetics," *SPE Journal*, Vol. 16, No. 8, August 1960, pp. 810–814.

6. Grassie, N., and Melville, H. W., "Thermal Degradation of Polymethylmethacrylate," *Bulletin des Societes Chimiques Belges*, Vol. 57, 1948, pp. 142–153.

7. Madorsky, S. L., "Rates and Activation Energies of Thermal Degradation of Styrene and Acrylate Polymers in a Vacuum," *Journal of Polymer Science*, Vol. 11, November 1953, pp. 491–506.

8. Bresler, S. E., Osminskaia, A. T., Popov, A. G., Saminskii, E. M., and Frenkel, S. Ia., "Thermal Degradation of Polymethyl Methacrylate," *Colloid Journal*, Vol. 20, 1958, pp. 381–392.

9. Straus, S., and Madorsky, S. L., "Pyrolysis of Styrene, Acrylate, and Isoprene Polymers in a Vacuum," Research Paper RP205, *Journal of Research, National Bureau of Standards*, Vol. 52, March 1953, pp. 165–176.

10. Madorsky, S. L., and Straus, S., *Thermal Degradation Studies of Polymers at High Temperatures*, Part III, WADC TR 59-64, Wright Air Development Center, Wright-Patterson AFB, Ohio, June 1961.

11. Goldsmith, A., Waterman, T. E., and Hirschorn, H. J., *Thermophysical Properties of Solid Materials. Vol. IV. Cermets, Intermetallics, Polymerics, and Composites*, WADC TR 58-476, Wright Air Development Center, Wright-Patterson AFB, Ohio, November 1960.

12. *Research Summary No. 36-8*, Jet Propulsion Laboratory, Pasadena, May 1, 1961, pp. 91–92.

13. Siegle, J. C., and Muus, L. T., *Pyrolysis of Polytetrafluoroethylene*, Polychemicals Department, E. I. du Pont de Nemours and Company, Inc., Wilmington, Delaware. Paper presented at meeting of the American Chemical Society, September 17, 1956.

14. Siegle, J. C., Muus, L. T., Lin, T. P., and Larsen, H. A., *The Molecular Structure of Pefluorocarbon Polymers. II. Pyrolysis of Polytetrafluoroethylene*, Polychemicals Department, E. I. du Pont de Nemours and Company, Inc., Wilmington, Delaware.

15. Starkweather, H. W., Jr., and Boyd, R. H., "The Entropy of Melting of Some Linear Polymers," *Journal of Physical Chemistry*, Vol. 64, April 1960, pp. 410–414.

REFERENCES (Cont'd)

16. Madorsky, S. L., Hart, V. E., Straus, S., and Sedlak, V. A., "Thermal Degradation of Tetrafluoroethylene and Hydrofluoroethylene Polymers in a Vacuum," Research Paper RP2461, *Journal of Research, National Bureau of Standards,* Vol. 52, December 1953, pp. 327–333.

17. Settlage, P. H., and Siegle, J. C., "Behavior of Teflon Fluorocarbon Resins at Elevated Temperatures," *Physical Chemistry in Aerodynamics and Space Flight,* proceedings of a conference held September 1–3, 1959, at the University of Pennsylvania. Pergamon Press, New York, 1961.

18. Marx, P., and Dole, M., "Specific Heat of Synthetic High Polymers. V. A Study of the Order–Disorder Transition in Polytetrafluoroethylene," *Journal of the American Chemical Society,* Vol. 77, September 1955, pp. 4771–4774.

19. Wentink, T., Jr., *High Temperature Behavior of Teflon,* Research Report R-55, Everett Research Laboratory, Avco Corporation, Everett, Massachusetts, July 1959.

20. Oakes, W. G., and Richards, R. B., "The Thermal Degradation of Ethylene Polymers," *Journal of the Chemical Society (London),* Part 4, 1949, pp. 2929–2935.

21. Jellinek, H. H. G., "Thermal Degradation of Polystyrene and Polyethylene," *Journal of Polymer Science,* Vol. 4, 1949, pp. 13–36.

22. Madorsky, S. L., "Rates of Thermal Degradation of Polystyrene and Polyethylene in a Vacuum," *Journal of Polymer Science,* Vol. 9, 1952, pp. 133–140.

23. Baramboim, N. K., and Sviridova, V. A., "Degradation of Low-Pressure Polyethylene," *High Molecular Weight Compounds,* Vol. 2, 1960 (in Russian), pp. 1193–1195.

24. Matsuoka, S., "The Effect of Pressure and Temperature on the Specific Volume of Polyethylene," *Journal of Polymer Science,* Vol. 57, 1962, pp. 569–588.

25. Dole, M., Hettinger, W. P., Jr., Larson, N. R., and Wethington, J. A., Jr., "Specific Heat of Synthetic High Polymers. I. A Study of Polyethylene Including a Statistical Theory of Crystallite Length," *Journal of Chemical Physics,* Vol 20, May 1952, pp. 781–790.

26. Madorsky, S. L., Straus, S., Thompson, D., and Williamson, L., "Pyrolysis of Polyisobutene (Vistanex), Polyisoprene, Polybutadiene, GR-S, and Polyethylene in a High Vacuum," Research Paper RP1989, *Journal of Research, National Bureau of Standards,* Vol. 42, May 1949, pp. 499–514.